Similarity Laws of Friction-Reduced Flows

W. B. GILES*
General Electric Company, Schenectady, New York

Similarity laws are developed and tested for the case of friction-reduced flows at minimum friction conditions using solvent-based Reynolds numbers. These laws are deduced from empirical pipe data and a modified $1/n$th-power velocity distribution that can describe both laminar and turbulent Newtonian flows. Integral momentum methods are used to test these laws in comparison with torque measurements on a rotating disk and displacement thickness measurements in the entry region of a pipe. The results of experiments in the entry region of a $1\frac{1}{4}$-in.-diam by 18-ft pipe are reported at water-based Reynolds numbers up to 9×10^5 and show friction reductions of 84%. Developing boundary-layer conditions are shown that simulate full-scale torpedo operation; and causes of suboptimum performance of large pipes and underwater vehicles are indicated.

Nomenclature

a = tube or disk radius
b = plate width
c = disk boundary-layer constant
C_f = $D/\frac{1}{2}2\rho U_\infty^2 bl$, flat plate friction coefficient
C_M = $2M/\frac{1}{2}\rho\omega^2 a^5$, disk friction
d = tube diameter
d/dx = total derivative with x
D = plate drag
H = δ^*/θ, profile shape parameter
l = plate length
M = disk moment
n = power law coefficient
p = local static pressure
r = radial coordinate
R_d = $\bar{u}d/\nu$, diametral Reynolds number
R_x = Ux/ν, length Reynolds number
$R_{x\text{crit}}$ = transition length Reynolds number
R_δ = $U\delta/\nu$, boundary-layer thickness Reynolds number
R_{δ^*} = $U\delta^*/\nu$, displacement thickness Reynolds number
R_ω = $a^2\omega/\nu$, disk Reynolds number
u = local axial velocity (tube), radial velocity (disk)
$\bar{u}$ = average velocity
u_0 = maximum radial velocity (disk)
U = maximum or freestream velocity
U_r = relative velocity (disk)
v = local tangential velocity
v_* = $(\tau_0/\rho)^{1/2}$, friction velocity
x = axial coordinate
y = coordinate normal to tube wall
α, β = empirical friction law coefficients
γ = $[(2 + H)/H]/[(2\delta^*/a)/(1 - 2\delta^*/a)]$
Γ = see Eq. (26)
δ = boundary-layer thickness
δ^* = displacement thickness
ϵ = δ/a
η = y/δ
θ = momentum thickness
κ = $\bar{u}/U$, average-to-maximum velocity ratio
λ = $8\tau_0/\frac{1}{2}\rho\bar{u}^2$, pipe friction coefficient
ρ = mass density
σ = empirical constant, $u_0 = \sigma r\omega$
τ = shear stress
ν = kinematic viscosity
φ = disk coordinate, Fig. 11
ω = rotation speed
$\partial/\partial r$ = partial derivative with r

Subscripts

o = wall conditions
r = radial component
t = tangential component
∞ = freestream conditions

Introduction

ONE of the most intriguing developments for improved underwater propulsion is the marked friction reduction of dilute solutions of high molecular weight, linear polymers. This phenomenon was first reported by Toms[1] in 1948, using polymethyl-methacrylate in monochlorobenzene. However, the potential of this technique appears to have been overlooked until the early 1960's when water-soluble polymers were studied for application to marine systems.

Dodge and Metzner[2,3] have shown that power law fluids can account for pressure drop reduction in pipes where the fluid is shear thinning or pseudoplastic. However, much more pronounced effects of friction reduction are generally ascribed to viscoelastic fluids.[4] Here friction reduction is evidenced even with reference to solvent-based Reynolds numbers and with fluid systems that have substantially Newtonian stress strain rate characteristics.

The mechanism involved appears to be largely one of enhanced flow stabilization in the presence of a wall through the action of the polymeric molecules. This can occur in the presence of turbulence, e.g., thickened laminar sublayer,[5] or can result in the complete suppression of turbulence.[6]

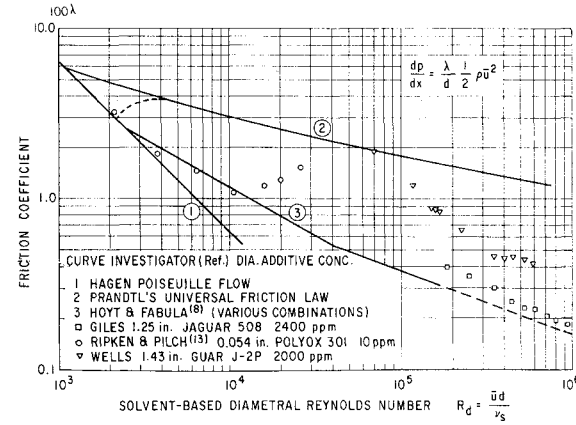

Fig. 1 Minimum pipe resistance of friction-reduced flow.

Presented as Paper 67-485 at the AIAA 3rd Propulsion Joint Specialist Conference, Washington, D. C., July 17–21, 1967; submitted August 3, 1967; revision received October 13, 1967.

* Project Engineer, Research and Development Center. Member AIAA.

Currently, considerable data are available with different types of additives, concentrations, and flow geometry. This work includes studies with capillaries and pipes,[7] rotating disks[8] and cylinders,[9] jets,[10] diffusers,[11] blunt bodies,[12] and test vehicles. In general, however, there are insufficient data on flat plates with which to relate to vehicle test data. Furthermore, with the increase in test variables there is a considerable variation in results, particularly for large-diameter pipes.[13] Hoyt and Fabula,[8] and others, have found a lower limit or minimum friction factor for both pipe and rotating disk flows, and further observed that this lower limit is the same for different, effective polymers and that it also correlates on a solvent-based Reynolds number.

The purpose of this paper is to identify the similarity laws for the condition of minimum friction and to further test their validity through investigations of the boundary-layer development in the entry region of a pipe.

Pipe-Flow Data

Figure 1 shows the minimum pipe resistance (curve 3) reported by Hoyt and Fabula[8] for various additives in water with pipe diameters of 0.043, 0.18, and 0.418 in. up to a water-based Reynolds number of 1.6×10^5, in comparison with Hagen-Poiseuille flow and Prandtl's universal friction law. Other investigators have achieved comparative values of minimum friction factors. For example, Pruitt and Crawford[14] report a maximum friction reduction of 80% of the difference between turbulent and laminar flow. Representative data of Ripken and Pilch[13] show close agreement with Hoyt and Fabula and also indicate that the minimum friction condition represents a modified laminar flow with delayed transition occurring at a Reynolds number of 1.2×10^4. Therefore, nonoptimum flow conditions can result from too low a polymer concentration (e.g., resulting in turbulence) or excessive concentrations (high viscosity). With small tubes and capillaries, the minimum friction conditions are readily achieved by different investigators and find agreement. However, with large pipes at high Reynolds number, such optimum flow conditions may not be as readily obtained. For example, high Reynolds number data by Wells[5] are compared with the minimum obtained in this study.

Similarity Law Development

From the empirical pipe data at minimum friction resistance, a new Blasius law of friction is determined and may be expressed in terms of the friction velocity $v_* = (\tau_o/\rho)^{1/2}$ or

$$\lambda \equiv 8(v_*/\bar{u})^2 = \beta(\bar{u}d/\nu)^{-\alpha} \qquad (1)$$

where $\beta = 2.18$, $\alpha = 0.5675$ for $R_d < 4 \times 10^4$, and $\beta = 0.2725$, $\alpha = 0.371$ for $R_d > 4 \times 10^4$.† Following Prandtl, (Ref. 15, p. 506) an expression for the maximum velocity is obtained in the form

$$U/v_* = (1/\kappa)[(8/\beta)2^\alpha]^{1/(2-\alpha)}(v_* a/\nu)^{\alpha/(2-\alpha)} \qquad (2)$$

where $\bar{u}/U \equiv \kappa$ and $d \equiv 2a$. Assuming that this expression holds for any velocity u at a position y from the wall results in the $1/n$th-power velocity distribution,

$$u/U = (y/a)^{1/n} \qquad n = (2 - \alpha)/\alpha \qquad (3)$$

This deduction of the turbulent velocity profile by Prandtl has been superseded by the inner law (or law of the wall), the outer law (or velocity defect law), and the logarithmic velocity law to better describe the laminar sublayer, turbulent, and buffer regimes, respectively. However, the simple $1/n$th-power velocity distribution is adequate for integral momentum methods at large values of n. In application to friction-reduced flows, low values of n are predicted, and in the limit of laminar Newtonian flow, $n = 1$, Prandtl's method yields a linear rather than a parabolic distribution. To overcome this defect, a velocity distribution is assumed that is compatible with both laminar and turbulent Newtonian flow and is then applied to the intermediate case of friction-reduced flow.

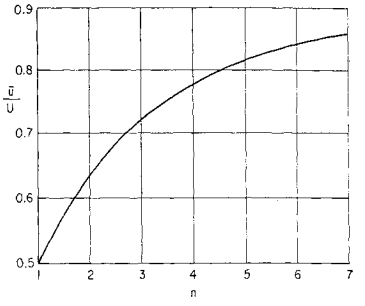

Fig. 2 Average to maximum velocity ratio as a function of profile shape.

Considering the form

$$u/U = [1 - (r/a)^{(1+n)/n}]^{1/n} \qquad r = a - y \qquad (4)$$

it is seen that the parabolic form for Hagen-Poiseuille flow is obtained exactly for $n = 1$. Expressing in terms of y from the wall and expanding‡ gives

$$\frac{u}{U} = \left(\frac{1+n}{n}\frac{y}{a}\right)^{1/n}\left[1 - \frac{1}{2n}\frac{y}{a} + \frac{1-n}{6n^2} \times \left(\frac{y}{a}\right)^2 + \ldots\right]^{1/n} \qquad (5)$$

or, for the turbulent Newtonian case of $n = 7$,

$$\frac{u}{U} = \left(\frac{8}{7}\frac{y}{a}\right)^{1/7}\left[1 - \frac{1}{14}\frac{y}{a} - \frac{1}{49}\left(\frac{y}{a}\right)^2 + \ldots\right]^{1/7} \qquad (6)$$

This formulation indicates a slightly fuller profile than the simple form of Eq. (3), within 2%, and hence good agreement with Nikuradse's experiments (Ref. 15, p. 505) except near the wall where the contributions to the displacement and momentum thickness are small.

Integration of velocity profile, Eq. (4), over the pipe cross section yields

$$\frac{\bar{u}}{U} = \kappa = 2\left[\frac{1}{2} - \frac{1/n}{3 + 1/n} + \frac{1/n(1/n - 1)}{2(4 + 2/n)} - \frac{1/n(1/n - 1)(1/n - 2)}{6(5 + 3/n)} + \ldots\right] \qquad (7)$$

and the ratio of average to maximum velocity is shown in Fig. 2 as a function of n. Hence, the shear stress and velocity profiles similarity laws for the case of minimum frictional resistance, $n = 2.525$ for $\alpha = 0.5675$, are

$$\frac{\tau_o}{\rho U^2} = \frac{\beta}{8}\frac{\kappa^2}{(2\kappa)^\alpha}\left(\frac{\nu}{Ua}\right)^\alpha = 0.11\left(\frac{\nu}{Ua}\right)^{0.5675} \qquad (8)$$

and

$$\frac{u}{U} = 1.141\left(\frac{y}{a}\right)^{0.396}\left[1 - 0.198\frac{y}{a} - 0.04\left(\frac{y}{a}\right)^2 + \ldots\right]^{0.396} \qquad (9)$$

or

$$\frac{u}{v_*} = 5.35\left(\frac{v_* y}{a}\right)^{0.396}\left[1 - 0.198\frac{y}{a} - 0.04\left(\frac{y}{a}\right)^2 + \ldots\right]^{0.396} \qquad (10)$$

† These high Reynolds number data are subject to further verification to determine if they are minimal.

‡ This power series is convergent in the region of interest except at the boundary $y = a$ where u is known to be equal to U.

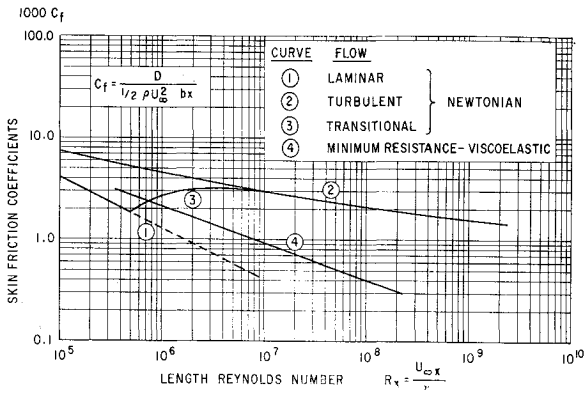

Fig. 3 Frictional resistance of flat plates.

Viscoelastic Flat Plate Flow

The development of the flat plate friction coefficient may now proceed on the basis of similarity with pipe flow, where the maximum velocity U_∞ exists at the boundary-layer thickness δ. From Eqs. (8) and (9),

$$\tau_o/\rho U_\infty^2 = (\beta/8)[\kappa^2/(2\kappa)^\alpha](\nu/U_\infty\delta)^\alpha \tag{11}$$

$$\frac{u}{U_\infty} = \left(\frac{1+n}{n}\frac{y}{\delta}\right)^{1/n}\left[1 - \frac{1}{2n}\frac{y}{\delta} + \frac{1-n}{6n^2}\left(\frac{y}{\delta}\right)^2 + \ldots\right]^{1/n} \tag{12}$$

and by definition, the displacement thickness δ^* and the momentum thickness θ are given by the expressions

$$\frac{\delta^*}{\delta} = \int_0^\infty \left(1 - \frac{u}{U_\infty}\right) d\frac{y}{\delta}$$
$$\frac{\theta}{\delta} = \int_0^\infty \frac{u}{U_\infty}\left(1 - \frac{u}{U_\infty}\right) d\frac{y}{\delta} \tag{13}$$

By numerical integration, for $n = 2.525$

$$\frac{\delta^*}{\delta} = 0.2336 \qquad \frac{\theta}{\delta} = 0.1346 \qquad \frac{\tau_o}{\rho U_\infty^2} = 0.11\left(\frac{\nu}{U_\infty\delta}\right)^{0.5675} \tag{14}$$

Since the flow over a flat plate in a zero pressure gradient is described by the solution to the differential equation

$$\tau_o/\rho U_\infty^2 = d\theta/dx \tag{15}$$

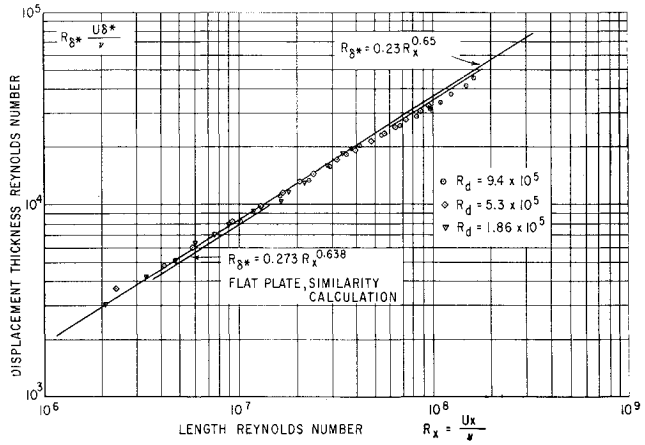

Fig. 4 Displacement thickness development in the entry region of 2400 ppm in water.

Table 1 Entry region flow parameters

ϵ	δ^*/a	θ/a	H	γ	Γ	$R_d^{0.5675}(d\delta/dx)$
0	0	0	1.735	0	0.1346	∞
0.05	0.01155	0.00663	1.745	0.0507	0.1417	6.21
0.1	0.02277	0.01300	1.750	0.102	0.1485	3.95
0.2	0.04438	0.02518	1.760	0.208	0.1613	2.39
0.3	0.0647	0.03645	1.775	0.316	0.1701	1.76
0.4	0.0840	0.04684	1.795	0.427	0.1803	1.37
0.5	0.1023	0.05640	1.815	0.540	0.1856	1.15
0.6	0.1190	0.06504	1.830	0.654	0.1893	0.987
0.7	0.1347	0.07287	1.850	0.767	0.1900	0.880
0.8	0.1495	0.07980	1.875	0.885	0.1884	0.802

and the total skin friction is given as

$$C_f = 2\frac{\theta}{l} = \frac{D}{\frac{1}{2}\rho U_\infty^2 b l} \tag{16}$$

then, for $n = 2.525$

$$\delta/x = 1.171R_x^{-0.362} \qquad \delta^*/x = 0.273R_x^{-0.362}$$
$$\theta/x = 0.1575R_x^{-0.362} \qquad C_f = 0.315R_x^{-0.362} \tag{17}$$

The skin-friction coefficient C_f is shown in Fig. 3, for both laminar and turbulent Newtonian flow, and the displacement thickness development, R_{δ^*} vs R_x, is shown in Fig. 4 with respect to experiments in a pipe entry region.

Entry Region of a Pipe

Following the same procedures, the flow in the pipe entry region may also be calculated. Here the integral momentum equation is expressed as

$$(dU^2\theta/dx) + U\delta^*(dU/dx) = \tau_0/\rho \tag{18}$$

and the displacement and momentum thicknesses are defined[16] with $\epsilon = \delta/a$ and $\eta = y/\delta$, so that the axisymmetric case converges to the two-dimensional case,

$$\frac{\delta^*}{\delta} = \int_0^1 \left(1 - \frac{u}{U}\right)(1 - \epsilon\eta)d\eta$$
$$\frac{\theta}{\delta} = \int_0^1 \frac{u}{U}\left(1 - \frac{u}{U}\right)(1 - \epsilon\eta)d\eta \tag{19}$$

Also, the continuity equation gives

$$U[1 - 2(\delta^*/a)] = \bar{u} \tag{20}$$

Now, by assuming the velocity profile§ for $n = 2.525$,

$$\delta^*/\delta = 0.2336 - 0.0585\epsilon \qquad \theta/\delta = 0.1346 - 0.0436\epsilon \tag{21}$$

and rearranging Eq. (18) in terms of $H = \delta^*/\theta$ and introducing the similarity law for wall stress,

$$\frac{d\theta}{dx} + \frac{2+H}{H}\frac{\delta^*}{U}\frac{dU}{dx} = \frac{\tau_o}{\rho U^2} = 0.11\left(\frac{\nu}{U\delta}\right)^{0.5675} \tag{22}$$

The continuity equation gives

$$\frac{\delta^*}{U}\frac{dU}{dx} = \frac{2\delta^*/a}{1 - 2\delta^*/a}\frac{d\delta^*}{dx} \tag{23}$$

And also,

$$R_\delta = \frac{U\delta}{\nu} = \frac{1}{2}\frac{R_d(\delta/a)}{1 - 2(\delta^*/a)} \tag{24}$$

§ In this treatment, the velocity profile is assumed independent of the axial acceleration, but the effect of continuity on the shape factor H is retained.

Letting

$$\gamma = \frac{2 + H}{H} \frac{2(\delta^*/a)}{1 - 2(\delta^*/a)}$$

then

$$\frac{d\theta}{dx} + \gamma \frac{d\delta^*}{dx} = 0.11 \left[\frac{2[1 - 2(\delta^*/a)]}{R_d(\delta/a)}\right]^{0.5675} \quad (25)$$

This is reduced by Eq. (21) into a differential equation in δ for a particular value of R_d, or

$$\Gamma \frac{d\delta}{dx} = 0.11 \left[\frac{2[1 - 2(\delta^*/a)]}{R_d(\delta/a)}\right]^{0.5675} \quad (26)$$

where

$$\Gamma = [0.1346 + 0.2336\gamma - (0.0871 + 0.117\gamma)(\delta/a)]$$

The coefficients may be evaluated for different values of shown in Table 1. At small values of δ/a, the solution reduces the case of the flat plate; or

$$\frac{\delta}{a} = 1.507 \frac{(x/a)^{0.638}}{R_d^{0.362}}$$

A sample solution of the displacement thickness development for $R_d = 5.4 \times 10^5$ is shown in Fig. 5 in comparison with the flat plate calculation, indicating that the pipe entry flow should act much like a flat plate in the test regime.

Entry Region Experimentation

The test facility consisted of a circulating-flow loop supplying a Lexan® tube (1.2467 ± 0.0005 in. in diam., 18.65 ft long) with a 10 to 1 contraction area inlet nozzle and a 24-in.-long conical diffuser (3° 22′ half-angle). The axial pressure distribution was measured by means of manometer taps spaced 8 in. apart and commencing 5.5 in. downstream of the nozzle. Flow was measured by differential pressure across the inlet nozzle which was calibrated with a turbine-type flow meter. The manometer bank data were recorded photographically to minimize errors due to time variations. This test facility is shown in the photograph of Fig. 6. With an accurate measurement of the tube bore and axial pressure distribution, the displacement thickness development and freestream acceleration may be determined directly from its definition for undeveloped flow [Eq. (20)]. For fully developed flow, λ and R_d are determined in a normal fashion.

Velocity profile traverses were also conducted, with a 0.021-in.-o.d., 0.010-in.-i.d. pitot tube brazed at $\frac{5}{32}$ in. from the end of a 0.059-in.-o.d. hypodermic tube inserted directly through

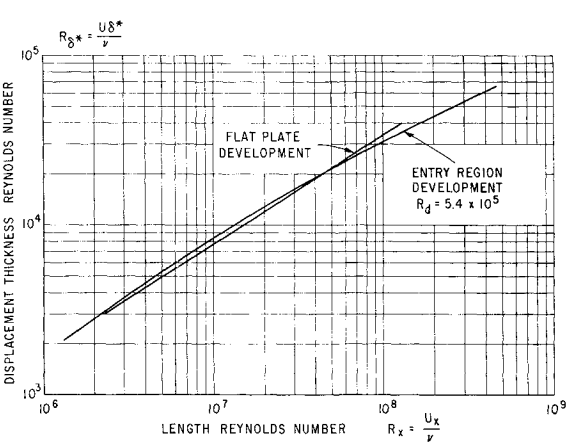

Fig. 5 Comparison of flat plate and entry region displacement thickness development for friction-reduced flow.

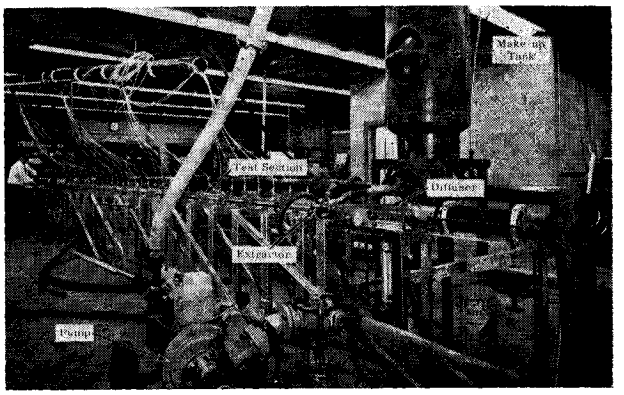

Fig. 6 Boundary-layer test facility.

the 0.070-in. pressure taps. Local static pressure was measured by extrapolation from the two upstream and two downstream pressure taps.

Solutions of guar gum (Jaguar 508, Stein Hall) were premixed at various concentrations and inserted into the test loop. In general, no shear or biological degradation¶ occurred during testing. The guar gum concentrations were varied to obtain minimum frictional resistance and the resulting values of λ vs R_d are summarized in Fig. 7 together with water data used for calibration. It must be noted that both 300 and 1200 ppm concentrations result in fully developed flow, while at 2400 ppm the flow was undeveloped over most of the test length with a rapid transition to fully developed flow. As a consequence, two friction factors are shown. At 4800 ppm, the flow was undeveloped over the whole test length and only the asymptotic, or downstream, values of λ are reported. It is evident, then, that concentrations near 2400 ppm represent minimum friction conditions, with lower concentrations resulting in early transition and higher concentrations resulting in laminar flow at excessive viscosity.

This entry region effect at minimum frictional resistance is shown in Fig. 8 as static pressure drop normalized with kinetic head, $\Delta p/\frac{1}{2}\rho\bar{u}^2$ vs the entrance length parameter x/dR_d, and is compared with fully developed laminar and turbulence flow and with laminar entry region flow for Newtonian flows, after Shapiro et al.[17] It is seen that the viscoelastic flow data also exhibit a strong entry region effect akin

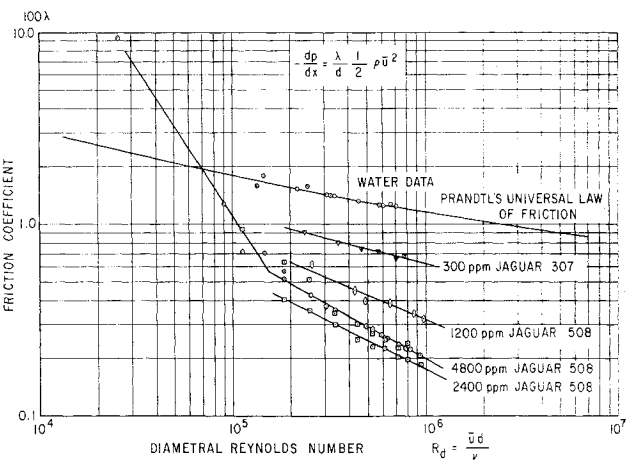

Fig. 7 Friction resistance of friction-reduced flow in a smooth pipe.

¶ Overnight storage of the test solution would exhibit biological degradation that could be suppressed by adding phenylmercuric acetate. Also some shear degradation was evident during the velocity profile traverses (slight upstream shift of the fully developed flow point) because of the much longer times of operation.

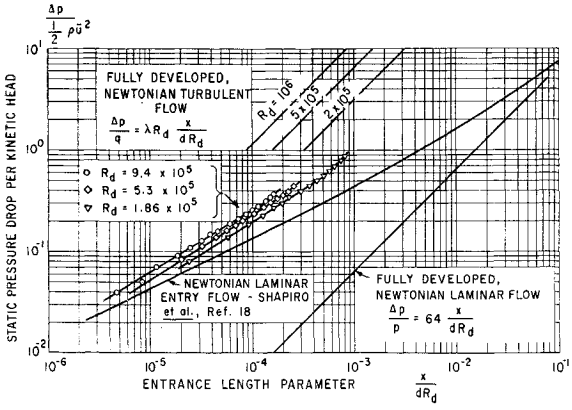

Fig. 8 Entry region effects of 2400 ppm Jaguar 508 in water.

to laminar Newtonian entry region flow in a region, $x/dR_d < 10^{-3}$, where the boundary-layer development in the pipe entry region is essentially the same as on a flat plate.

Figure 4 shows the same data reduced to the form of local displacement thickness and length Reynolds numbers, R_{δ^*} and R_x, respectively. These data now show complete correlation and excellent agreement with similarity prediction of both the flat plate and pipe entry region flows of viscoelastic fluids.

In Fig. 9, the static pressure drop data $\Delta p/\frac{1}{2}p\bar{u}^2$ are shown correlated in terms of the viscoelastic entrance parameter $x/dR_d^{0.5675}$ and are compared with the similarity prediction in the entry region for $R_d = 5.4 \times 10^5$ and fully developed flow, using $\lambda = 2.18R_d^{-0.5675}$. The results of a pitot tube traverse are shown in Fig. 10 together with fully turbulent water data. These data** were taken downstream, $x/l = 133.0$, at $R_d = 5.4 \times 10^5$, where the flow has just gone into transition and is fully developed according to axial pressure measurements. The flow in this region is seen to be turbulent with a greatly thickened laminar sublayer. It is of interest to note that the laminar sublayer tends to fit a form predicted by similarity, or

$$u/v_* = 5.35(v_* y/\nu)^{0.396}$$

exclusive of the point 0.005 in. from the wall.

Integration of the pitot tube traverse resulted in an indicated average velocity of 8.5% less than the actual average velocity of 50.4 fps. This variance is significantly less than

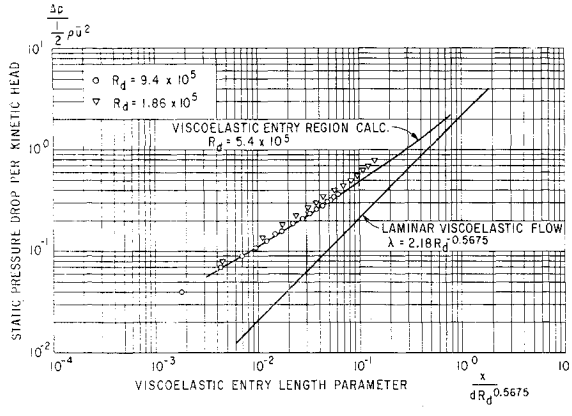

Fig. 9 Entry region correlation of 2400 ppm Jaguar 508 in water.

** The data were corrected for the blockage induced by the pitot tube (2.5% maximum) and correlated with a friction velocity v^*, determined from the two upstream manometer taps, the average over the two upstream and two downstream taps, and also from Fig. 7, as represented by the upper data of 2400 ppm.

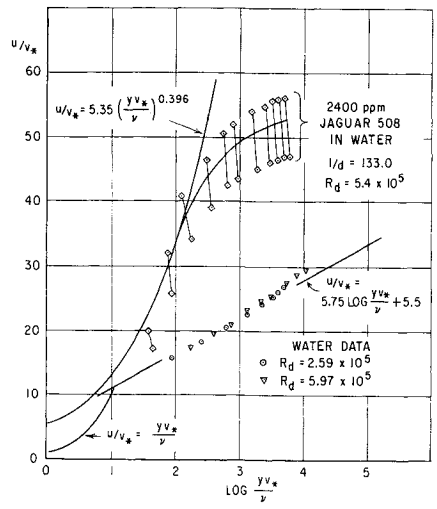

Fig. 10 Pitot tube traverses.

those reported by Astrarita and Nicodemo[18] which are attributed to the influence of normal stresses.

With the agreement indicated between similarity prediction of minimum friction viscoelastic flow and experimentation, the question of transition may now be considered. Table 2 tabulates the critical local-length Reynolds number (determined as the point of transition to fully developed turbulent flow) with respect to local velocity, displacement thickness, and boundary layer thickness. Since $\delta/a < 1$ and the entry region flow does not asymptotically approach the fully developed flow, it is concluded that these points represent transition to turbulence in the undeveloped boundary layer and are approximately two orders of magnitude greater than experienced with Newtonian flow. Furthermore, the strong dependence of critical Reynolds numbers on velocity suggests that the stability of laminar viscoelastic flow is also heavily dependent on a favorable pressure gradient, as with Newtonian flow. Pipe testing with sudden contraction inlets or blunt nose vehicles would, therefore, be expected to inhibit the achievement of minimum friction conditions.

Rotating Disk Flow

A further test of the validity of the viscoelastic similarity laws is provided by comparison with rotating disk experiments. This experiment avoids the influence of pressure gradient and wall curvature associated with pipe flow.

The solution follows in an analogous manner, after von Kármán.[19] With τ_r and τ_t the radial tangential stresses and u and v the radial and tangential velocities (see Fig. 11), the integral momentum equations are

$$-\frac{\tau_r}{\rho} r + \int_0^\delta v^2 dx = \frac{\partial}{\partial r} \int_0^\delta u^2 r dx$$

$$\frac{\tau_r}{\rho} r^2 = \frac{\partial}{\partial r} \int_0^\delta uvr^2 dx \qquad (27)$$

In consideration of the necessary boundary conditions,

$$u(0) = 0 \quad v(0) = r\omega \quad u(\delta) = 0 \quad v(\delta) = 0 \qquad (28)$$

Table 2 Transition data

$R_d \times 10^{-5}$	U, fps	δ^*/a	δ/a	$R_{x\text{crit}}$ 10^{-7}
1.12	14.3	0.138	0.71	1.44
1.87	22.5	0.114	0.57	2.12
3.35	38.0	0.091	0.44	3.65
5.32	60.0	0.091	0.44	6.06
9.38	97.0	0.072	0.34	13.3

And taking the approximate, $1/n$th-power law velocity profile, then

$$u = u_0\left(\frac{x}{\delta}\right)^{1/n}\left(1 - \frac{x}{\delta}\right) \qquad v = r\omega\left[1 - \left(\frac{x}{\delta}\right)^{1/n}\right] \quad (29)$$

The velocities relative to and immediately adjacent to the disk produce the stresses and have a resultant magnitude of

$$U_r = [u_o^2 + (r\omega)^2](x/\delta)^{1/n}$$

and ' at an angle φ to the tangent. The stresses are, th ore,

$$\tau_r = \tau_o \sin\varphi = \tau_o\sigma/(1 + \sigma^2)^{1/2}$$

$$\tau_t = \tau_o \cos\varphi = \tau_o/(1 + \sigma^2)^{1/2}$$

where, $u_o = \sigma r\omega$. Now by similarity with pipe flow, Eq. (8), and with $n = 2.525$, the wall stress is

$$\tau_o/\rho U_\infty^2 = 0.091(\nu/U_\infty\delta)^{0.5675} \quad (30)$$

with $U_\infty = r\omega[1 + \sigma^2]^{1/2}$. The coefficient of this expression s adjusted to accommodate the use of the approximate, $1/n$th velocity profile, which requires that the displacement thickness be taken as 1/1.396 of the actual displacement thickness.

The shear stresses are thus

$$\tau_r = 0.091\rho(r\omega)^2(\nu/r\omega\delta)^{0.5675}\sigma[1 + \sigma^2]^{0.2162}$$
$$\tau_t = 0.091\rho(r\omega)^2(\nu/r\omega\delta)^{0.5675}[1 + \sigma^2]^{0.2162} \quad (31)$$

Evaluation of the integrals of Eq. (27) for $n = 2.525$ gives

$$\int_0^\delta v^2dx = 0.124(r\omega)^2\delta$$

$$\frac{\partial}{\partial r}\int_0^\delta u^2rdx = 0.108\sigma^2\omega^2\frac{dr}{d}(r^3\delta) \quad (32)$$

$$\frac{\partial}{\partial r}\int_0^\delta uvr^2dx = 0.10\sigma\omega^2\frac{d}{dr}(r^4\delta)$$

Substituting Eqs. (31) and (32) into the integral momentum equations will result in two simultaneous differential equations that may be solved explicitly for σ and $\delta(r)$. However, a simpler procedure is to deduce the form of δ. Namely, noting that the radial stress must balance the centrifugal force on an element of height δ of the boundary layer, $\tau_o \sin\varphi = \rho\omega^2r\delta$, and from Eq. (31)

$$\tau_o \cos\varphi \approx \rho(r\omega)^2(\nu/r\omega\delta)^{0.5675}$$

Therefore,

$$\delta = cr^{0.276}(\nu/\omega)^{0.362} \quad (33)$$

Substituting into Eqs. (28) results in the expressions

$$0.091\sigma[1 + \sigma^2]^{0.2162} = [0.124 - 0.354\sigma^2]c^{1.5675}$$

$$0.091[1 + \sigma^2]^{0.2162} = 0.4276\sigma c^{1.5675}$$

which yield $\sigma = 0.398$ and $c = 0.685$. Integrating again for

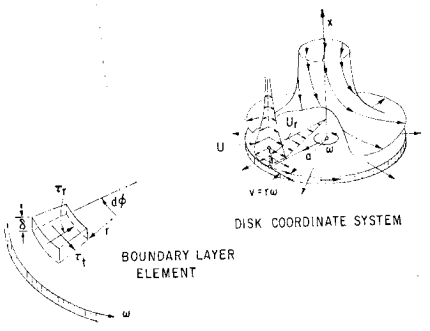

Fig. 11 Flow in the neighborhood of a rotating disk.

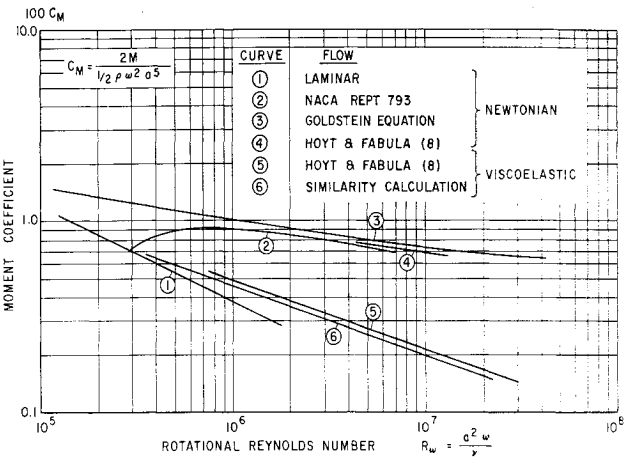

Fig. 12 Frictional resistance of rotating disk.

the total torque M on the disk face yields

$$M = 2\pi\int_0^a r^2\tau_t dr = 2\pi\rho a^2\int_0^\delta uvdx$$

$$= 0.171\rho\omega^2a^5\left(\frac{\nu}{a^2\omega}\right)^{0.362}$$

With a disk wetted on both sides, the moment coefficient is defined as

$$C_M = \frac{2M}{\frac{1}{2}\rho\omega^2a^5}$$

Therefore, the minimum friction condition for viscoelastic flow on a rotating disk is

$$C_M = 0.684R_\omega^{-0.362} \qquad R_\omega = a^2\omega/\nu \quad (34)$$

The result is shown in Fig. 12 in comparison with the data of Hoyt and Fabula. The relatively small discrepancy, approximately 8%, could be due to tip losses in the experiment.

Conclusions

This study indicates that the minimum friction condition of friction-reduced flow in pipes and capillaries, in the pipe entry region, and on rotating disks are mutually compatible through similarity transformations, based solely on an empirically defined law of friction and analytically treated by standard Newtonian methods.

This correlation also indicates the validity of the flat plate equations, up to length Reynolds numbers of 10^8, based on the pipe entry region experiments where $\delta < a$. Because of the agreement obtained with both entry region and rotating disk flows, the effects of acceleration on the velocity-profile shape factor and wall curvature appear to be of negligible importance in the determination of the boundary layer and wall friction. However, the experiments also suggest that acceleration could be a significant factor in enhancing flow stability; or conversely, that sudden contraction inlets or blunt-nosed vehicles could force early transition from the modified flow (minimum friction) into turbulent flow.

References

[1] Toms, A. B., *Proceedings of the International Congress of Rheology 1948*, Vol. II, North Holland Publishing, Amsterdam, 1949, p. 135.

[2] Dodge, D. W. and Metzner, A. B., *Rheologica Acta*, Vol. 1, Aug. 1958, p. 205 (cf. p. 65 of Ref. 3).

[3] Wilkinson, W. K., *Non-Newtonian Fluids, Fluid Mechanics, Mixing, and Heat Transfer*, Pergamon Press, 1960.

[4] Metzner, A. B., "Flow of Non-Newtonian Fluids," Sec. 7, *Handbook of Fluid Dynamics*, edited by V. L. Streeter, McGraw-Hill, New York, 1961.

[5] Wells, C. S., Jr., "On the Turbulent Shear Flow of an Elastico-Viscous Fluid," Paper 64–36, 1964, AIAA; also *AIAA Journal*, Vol. 3, No. 10, Oct. 1965, pp. 1800–1805.

[6] Giles, W. B., "Laminar Viscoelastic Boundary Layers with Roughness," Rept. 64GL51, March 11, 1964, General Electric Co.

[7] Fabula, A. G., "The Toms Phenomenon in the Turbulent Flow of Very Dilute Solutions," *Proceedings Fourth International Congress of Rheology*, Part 3, Interscience, New York, 1965, pp. 455–479.

[8] Hoyt, J. W. and Fabula, A. G., "The Effect of Additives on Fluid Friction," NAVWEPS Rept. 8636, ASTIA AD 612 056, Dec. 1964, Naval Ordnance Test Station, China Lake, Calif.

[9] Shin, H., "Reduction of Drag in Turbulence by Dilute Polymer Solutions," Doctoral thesis, June 1965, Massachusetts Institute of Technology; also *Transactions of the Rheological Society*, Vol. 10, 1966, pp. 335–351.

[10] Gadd, G. E., "Turbulence Damping and Drag Reduction Produced by Certain Additives in Water," *Nature*, May 1, 1965, pp. 463–467.

[11] Patrick, H. V. L., "The Effect of High Molecular Weight Polymer Additives on the Performance of a Conical Diffuser," Paper 66-658, June 1966, AIAA.

[12] Lang, T. G., "Drag of Blunt Bodies in Polymer Solutions, 66-WA/FE-33, 1966, American Society of Mechanical Engineers New York.

[13] Ripken, J. F. and Pilch, M., "Non-Newtonian Pipe Friction Studies with Various Dilute Polymer Water Solutions," Rept. 71 BuShips Contract S-R009-01-01, June 1964, St. Anthony Fall Hydrodynamics Lab., University of Minnesota.

[14] Pruitt, G. T. and Crawford, H. R., "Effect of Molecular Weight and Segmental Constitution on the Drag Reduction of Water Soluble Polymers," DTMB Contract NONR-4306(00) ASTIA AD 625 801, April 1965, The Western Co.

[15] Schlichting, H., *Boundary Layer Theory*, 4th ed., McGraw Hill, New York, 1960, pp. 505, 506.

[16] Ross, D., "Turbulent Flow in the Entrance Region of Pipe," Paper 54-H-89, 1954, American Society of Mechanical Engineers, New York.

[17] Shapiro, A. H., Siegel, R., and Kline, S. J., "Friction Factor in the Laminar Entry Region of a Smooth Tube," *Proceedings 2nd National Congress of Applied Mechanics*, 1954, American Society of Mechanical Engineers, New York.

[18] Astarita, G. and Nicodemo, L., "Velocity Distributions and Normal Stresses in Viscoelastic Turbulent Pipe Flow," *AIChE Journal*, Vol. 12, No. 3, May 1966, pp. 478–483.

[19] von Kármán, T., "On Laminar and Turbulent Friction," TM1093, Sept. 1946, NACA; also *Zeitschrift fur Mathematik und Mechanik*, Vol. 1, No. 4, Aug. 1921.

JANUARY 1968 J. HYDRONAUTICS VOL. 2, NO.

Deep Ocean Work Boat (DOWB), an Advanced Deep Submergence Vehicle

SCOTT C. DAUBIN*

AC Electronics, Division of General Motors Corporation, Santa Barbara, Calif.

The submarine will carry two persons to depths of 6500 ft, there to observe and to do work. The spherical pressure hull of HY 100 steel, 82 in. o.d. by 0.935 in. thick is machined inside and out. Spherical symmetry is broken only in hatch areas at the north and south poles. A free flooding fiberglass fairing, 17 ft long by 8⅔ ft beam, mounts on pressure hull. The fairing provides a smooth form and contains ballast systems, the propulsion system, manipulator, TV cameras, transducers, and miscellaneous instruments. A cylindrical load skirt provides tie points for the fairing, supports the vehicle when out of water and supports the main batteries. Surface displacement is 16,295 lb; metacentric height is 13 in. surfaced and 5 in. submerged. Lead acid batteries provide 40 kwh of main power. Propulsion drive system utilizes modulating solid-state inverters. An optical system provides pilot and observer full 4-pi solid angle visibility through 180-deg wide angle objectives mounted outboard of ports through hatches. A six-degree-of-freedom manipulator lifts a 50 lb weight at a 49 in. reach. The sonar system provides search, terrain avoidance, upward and downward fathometers, underwater, telephone, and tracking beacon.

1. General

THE Deep Ocean Work Boat (DOWB) is a manned undersea vehicle designed to carry two men to depths of 6500 ft, there to do work as its name implies. To carry out its mission it is equipped with an electromechanical manipulator and various viewing and sensing systems that permit it to operate in the black depths near obstacles and potential entanglements.

Presented as Paper 67-370 at the AIAA/SNAME Advanced Marine Vehicles Meeting, Norfolk, Va., May 22–24, 1967; submitted May 19, 1967; revision received October 16, 1967.

* Head, Marine Sciences Section, Sea Operations Department, Defense Research Laboratories.

The philosophy that underlay the design of DOWB aim at producing a large payload-payvolume-depth performa at the minimum expense in weight and size, which w limited by available surface support vessels and the requ ment for both highway and air transportability. Since, of the systems, the pressure hull consumes the single larg share of weight, in its design an attempt was made to minim weight; this was accomplished partly through simplicity the conservation of symmetry.

Table 1 outlines the principal operational characteristi Figures 1–4 show the general plane. DOWB's configuratio that of a spherical pressure hull surrounded by a free flood fiberglass fairing. The prolate spheroid form of the fair is interrupted by the cylindrical main ballast tank penetra